Undergraduate Thesis Report

GEOL 543

Department of Geological Sciences and Geological Engineering

Queen's University, Kingston

Estimating Fundamental Site Frequency and Soil Thickness using the Horizontal to Vertical Spectral Ratio Method on Wolfe Island, Ontario

Author:
Dean Bucciarelli

Supervisors:
Dr. Hom Nath Gharti
Dr. Alexander Braun

April 19, 2022

Acknowledgements

Abstract

Regional information on the soil thickness (h) and fundamental site frequency (f_0) are critical components for land-use planning and infrastructure development. In both urban and rural environments, civil engineers require an accurate estimation of both parameters to ensure the safety and longevity of structures. Traditional methods to determine soil thickness such as drilling are time-consuming, invasive and require a lot of manual labour. Conversely, collecting passive seismic data and analysing it using the Horizontal to Vertical Spectral Ratio (HVSR) method has proven to be an effective, fast, non-invasive and affordable means of estimating soil thickness and fundamental site frequency. By recording seismic microtremors, and taking the ratio between the horizontal and vertical components of the Fourier amplitude spectra, it is possible to determine the fundamental site frequency. A combination of the fundamental site frequency and the average shear wave velocity of the soil layer (V_s) allows for the estimation of soil thickness. Approximations of the average shear wave velocity were determined via the 1D Multichannel Analysis of Surface Waves (MASW) method.

In this study, more than 50 recordings of passive microseismic data from nearly 20 locations on Wolfe Island, Ontario were collected and analysed with the HVSR technique. 43 microtremor recordings were found to produce clear and reliable fundamental site frequency peaks. Using this, estimates for soil thicknesses were made using an island-wide average shear wave velocity of the soil layer (250m/s). Soil thickness estimates were also made using site-specific average shear wave velocities of the soil layer as determined by available water well data. For recordings within 500m of a water well, it was found that using an island-wide average shear wave velocity resulted in soil thickness estimates within ~1m of the water well data. On the other hand, using a site-specific average shear wave velocity resulted in soil thickness estimates within

~0.4m of the water well data. Furthermore, the rate of data acquisition and processing led to the interest of many land-owners. This suggests the potential economic viability and usefulness of this method as a faster, more cost-effective and non-invasive alternative to drilling for estimations of the soil thickness where an exact value is not required.

Keywords:

- Fundamental site frequency

- Soil thickness

- Depth to bedrock

- Shear wave velocity

- Horizontal to Vertical Spectral Ratio (HVSR)

- Microtremor signal

Contents

Chapter 1

Introduction

1.1 Motivation

Proper understanding and characterization of the subsurface conditions and composition is a critical component of geotechnical design and planning, especially in infrastructure development and land-use planning. For nearly all site characterisation, information of the depth to bedrock or the thickness of the soil layer (h) and fundamental site frequency (f_0) are integral components. However, traditional methods of determining soil thickness such as drilling are; time-consuming, disruptive, labour-intensive and expensive. The development of microseismic survey methods (Aki 1957), has allowed for alternative non-invasive tools for geophysical exploration and studies. Popularised by Yutaka Nakamura (Nakamura 1989), the horizontal to vertical spectral ratio (HVSR) method enables the retrieval of shallow-subsurface seismic properties such as the fundamental site frequency for the site amplification effect (Nakamura 1989; Seht 1999; Mucciarelli 2001; Mucciarelli 2010; Xu 2021 and more). With knowledge on the average shear wave velocity (V_s) of the soil layer and the fundamental site frequency, an estimation of the soil thickness can be made. These properties can be obtained by measuring microtremors of the soil layer using a single three-component seismometer. This classifies the HVSR method as a passive and non-invasive technique, making it especially attractive to land-owners in urban and rural areas alike. Due to the relative ease of data acquisition and signal processing, this technique has gained significant popularity over the last quarter century (Mucciarelli 2001; Xu 2021; Tian 2019 and more).

In this report, the HVSR method will be used on Wolfe Island, Ontario, for a few key

reasons:

1. To contribute to non-existent public data on the fundamental site frequencies (f_0) of the soil layer on Wolfe Island.

2. To compare and test the accuracy and effectiveness of the non-invasive HVSR soil thickness (h) estimates to geotechnical data acquired via drilling.

3. To contribute site-specific estimations of soil thickness (h) on Wolfe Island to the public domain.

1.1.1   HVSR Theory and Applications

Nakamura first proposed the HVSR method for site effect studies, as a solution to the issues with traditional methods of using a reference site (Nakamura 1989; Xu 2021). Since then, the HVSR method has been used for a vast array of applications with varying degrees of success. It has been frequently used for site classification and site amplification studies which enables seismic risk assessment (Mucciarelli 2001; Mucciarelli 2011; Giannaraki 2019; Panzera 2019; Xu 2021; Yilar 2017; Tian 2019 and more). The method can also be usefully applied for inversion of shear wave velocity structure, mineral exploration, groundwater exploration, sedimentary basin characterisation, seasonal variability in soil layer and measuring fundamental resonance frequencies of buildings (Mucciarelli 2001; Xu 2021; Rigo 2021).

Despite the popularity of the method, a precise physical explanation of the derived results remains a moderately debated and controversial topic (Mucciarelli 2001; Xu 2021; Rigo 2021). Most of the debate is regarding the nature of the ambient seismic wave field and its source (Mucciarelli 2001; Xu 2021), where some believe it is dictated by shear wave resonance in the soil layer (Nakamura 1989; Seht 1999) and others believe it is due to the polarization effect of the fundamental surface waves (Lachet 1994; Bard 1998). The implications of a precise explanation depends on what the intended use of the HVSR method is. For example, it is commonly believed that the HVSR amplitude underestimates the site amplification effect (Mucciarelli 2001, Parolia 2012; Xu 2021, Rigo 2021, Tian 2019 and more). However, the literature is in widespread agreement that the HVSR method is an effective way to determine the fundamental site frequency (Mucciarelli 2001; Xu 2021; Rigo 2021; Seht 1999; Braganza 2016; Tian 2019; Nakamura

1989 and more). This report will thus only use the HVSR technique as a method to estimate the fundamental site frequency. This will then be used to estimate the soil thickness with the addition of external knowledge of the average shear wave velocity of the soil layer.
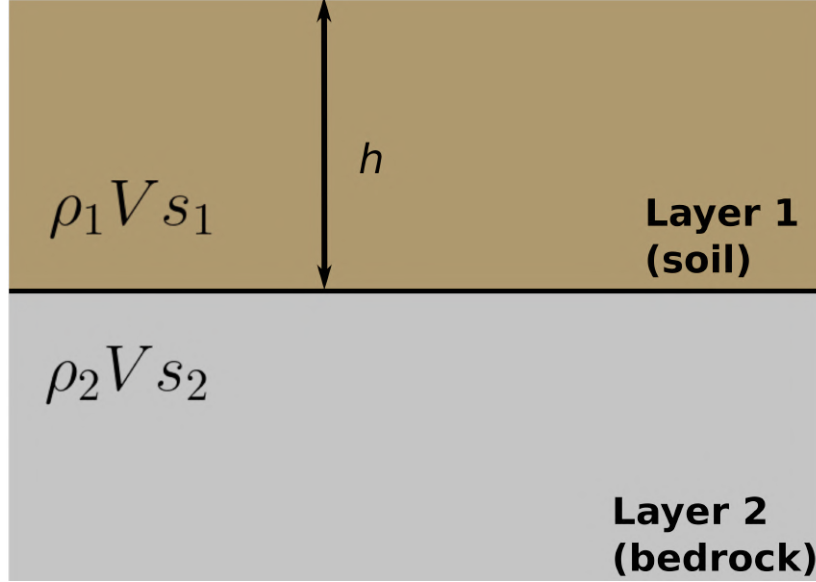
Figure 1.1 Conceptual two-layer Earth model necessary for the proper implementation of the HVSR technique. Vs_1 and Vs_2 represent the shear wave velocity of the soil and bedrock layers respectively. ρ_1, ρ_2 represent the density of the soil and bedrock layer respectively. This model assumes $Vs_2\rho_2 \geq Vs_1\rho_1$ such that $\frac{Vs_2\rho_2}{Vs_1\rho_1} \geq 2$. h is the thickness of the soil layer

For sites with a soft soil layer and an underlying hard and flat bedrock as seen in Figure(1.1), the basic principle of the HVSR method is summarised as follows: in a specific frequency band, the horizontal ground motion amplification is relatively magnified, whereas the vertical ground motion amplification is not significantly magnified (Mucciarelli 2001; Xu 2021; Nakamura 1989). An estimation of the fundamental (predominant) site frequency can thus be obtained by taking the ratio of the Fourier amplitude spectra of the horizontal and vertical components of ground motion. This is visualised in Figure(1.2(a)) where a gap between the horizontal and vertical components of the Fourier amplitude spectra is seen around 11Hz. Taking the ratio between these components will exaggerate the difference in the Fourier amplitude spectra, resulting in a clearly defined peak (at 11Hz) in the HVSR curve as seen in Figure(1.2(b)). This curve is representative of the predominant/fundamental site frequency, which can be expressed through the general relation (Seht 1999):

$$f_0 = \frac{V_s}{4h} \tag{1.1}$$

where V_s is the average shear wave velocity of the soil layer (in metres per second), h is the thickness of the soil layer or depth to bedrock (in metres), and f_0 is given in hertz. More generally, the seismic resonance frequency can be expressed as:

$$f_n = (2n+1)\frac{V_s}{4h} \tag{1.2}$$

where n is the resonance mode and the remaining variables are the same as Eq(1.1). Typically, a sites predominant resonant frequency occurs at the fundamental mode, leaving Eq(1.2) to be used much less frequently.
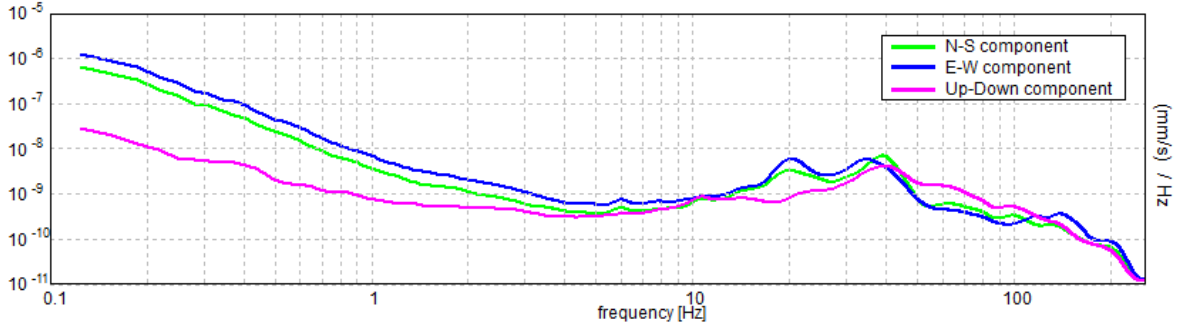
(a) Fourier amplitude spectra of ground motion for all three spatial dimensions
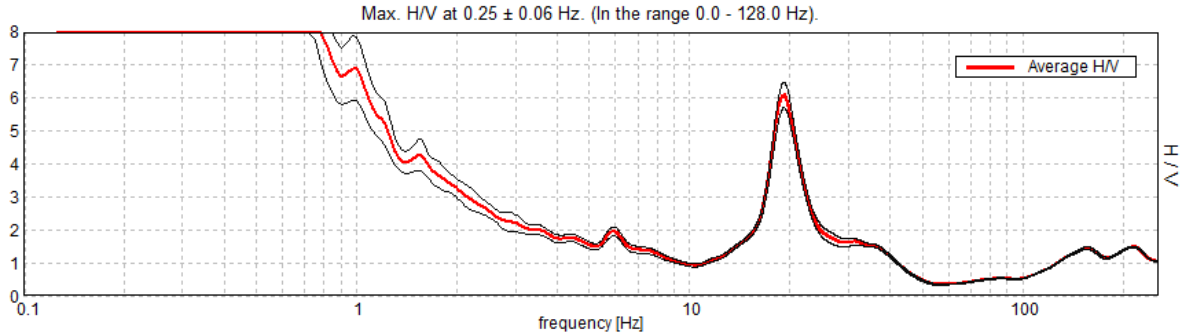
(b) HVSR curve obtained from Fourier Spectra in (a)

Figure 1.2 Visualisation of the basic mathematical formulation governing the HVSR technique.

1.1.2 Geological Setting

Wolfe Island is located in Lake Ontario at the entrance of the Saint Lawrence River. The island faces the Province of Ontario to the north. There are continuous ferry trips to and from Kingston which serves as the primary method of transportation to the mainland.

Wolfe Island also faces New York State to the south, with seasonal ferry trips to and from Cape Vincent. The island is a rural setting located within the Frontenac County with a permanent population of just under 1,500 residents.

A surficial geology map of Southern Ontario allows insight into key geological information of the soil layer, including but not limited to; geological formation, material type and surface area (Ontario Geological Survey 2004). Analysing only the Wolfe Island portion of the data, Figure(1.3) suggests that the majority of the island is covered by clay and silt, with the additional deposits of sand and gravel, muck and peat, bedrock drift complex and exposed regions of limestone bedrock. Additionally, the Ontario Ministry of the Environment, Conservation and Parks provides an extensive database of water well logs dating back to 1899, with approximately 20,000 additional well logs added annually (Ontario Ministry of the Environment, Conservation and Parks 1899-2021). There exists nearly 600 of such water wells on Wolfe Island, completed to varying degrees of accuracy and consistency. Over 90% of the analyzed records indicated clay as the primary material of the soil layer, with all of the records indicating limestone as the bedrock material. Using these two data sets as a guide, we can summarize the relevant geology as:

- Composition of soil layer: **Clay** (primarily)

- Composition of bedrock: **Limestone**

- Soil thickness range: **0-10m**

A brief comparison of typical shear wave velocities of both materials (L'Heureux 2017; Assefa 2002) allows for the confirmation that a sufficiently large impedance contrast exists between clay and limestone. This makes the geological setting of Wolfe Island ideal for the implementation of the HVSR technique.
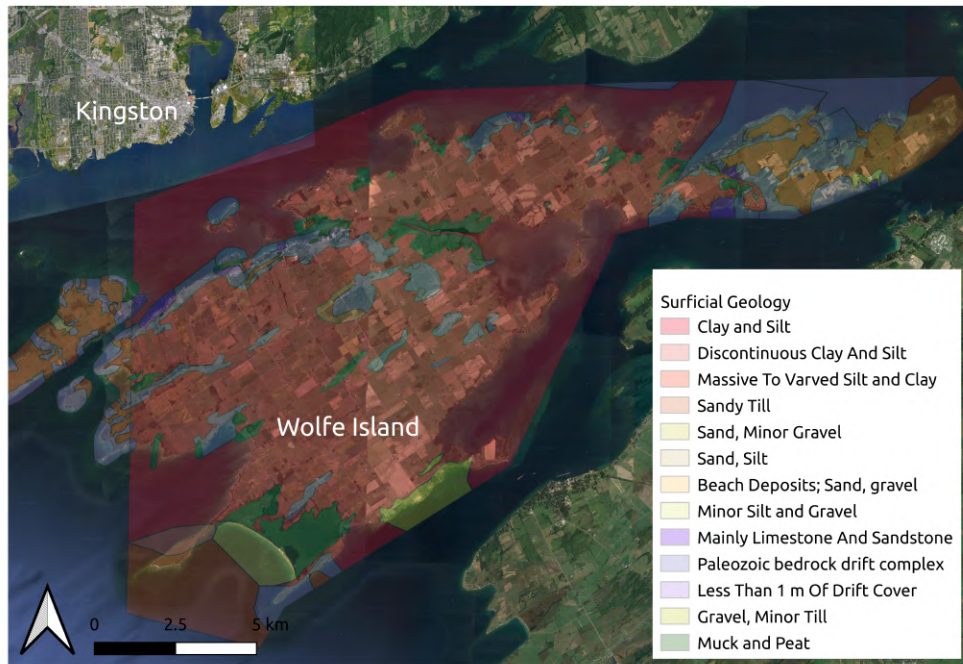
Figure 1.3 Surficial Geology of Wolfe Island. Ontario Geological Survey (2010).

Chapter 2

Methods

2.1 Data Acquisition

Two Tromino3G, three-component seismometers were used for all seismic recordings. Large buckets were flipped and used to cover the seismometrs from the prevalent winds on the island. Recordings were sampled at 512Hz for a duration of 10 minutes, with a minimum of two recordings per site as suggested by the literature (SESAME 2004).

| (a) | (b) |

Figure 2.1 (a) Close up of seismometer used. (b) Seismometer covered by bucket for wind protection.

2.2 Fundamental Site Frequency Calculation

2.2.1 Outline

No precise outline for the HVSR method was available for the first 15 years of its usage. This led to a vague HVSR recipe that was followed leading to several slight variations of the HVSR technique (Mucciarelli 2001). In 2004, with the contribution of nearly 100 participants from more than 15 European Institutions, the European Research Commission released *Guidelines for the Implementation of the H/V spectral Ratio Technique on Ambient Vibrations - Measurements, Processing and Interpretation* (SESAME 2004). This document now acts as the industry standard guidelines and is used in nearly every research article involving HVSR measurements published after 2004. As the title suggests, the document provides a wealth of detailed explanations and guidelines for accurate and effective data acquisition, processing and interpretation.

The basic HVSR process can be summarised into seven main steps:

1. **Collect ambient seismic data.**

2. **Window data to remove transients.** In other words, cut time signal into small segments in order to remove large ground movement induced by vehicles, footsteps and other unwanted anthropogenic sources.

3. **Filter or cut data**. Can be used if the user knows the frequency range of interest, otherwise not necessary and not always available. Variety of filters are possible, with a band-pass being the most common.

4. **Obtain Fourier amplitude spectra of each window.** Calculated via Fast Fourier Transforms (FFT).

5. **Smooth and average signals from separate windows.** Horizontal and vertical components must be treated separately.

6. **Take ratio between horizontal and vertical Fourier amplitude spectra.**

7. **Pick fundamental site frequency (f_0) and verify if reliability conditions are met.**

2.2.2 Conditions of Reliability

As mentioned, the SESAME European research project has provided extensive guidelines to ensure the proper interpretation of HVSR curve results. They created six conditions or criteria of reliability which are further broken down into three conditions of stability and three conditions of clarity. In this case, reliability implies stability (SESAME 2004), meaning that the HVSR curve obtained should be representative of HVSR curves that would be obtained using any other ambient vibration recording (ie, using a different device or measuring at a different time of day) and/or with other physically reasonable window selection. In other words, the HVSR results obtained should be easily reproducible for a given site. On the other hand, clarity is satisfied when the HVSR curve exhibits a clear, single peak. A detailed list of the conditions can be found in Chapter(5.3). If the HVSR curves for a given site satisfy *at least five out of the six conditions*, then the estimated fundamental site frequency can be considered to be very reliable.

2.2.3 Softwares

Two separate software packages were used to calculate HVSR curves in order to ensure accuracy and consistency of the calculated fundamental site frequency values from a single microtremor signal. First, *Grilla* is an integrated software package specifically designed to read, organize and analyse seismic records from Tromino seismometers. It allows the user a choice to manually select the desired windows, or have it done automatically where a specific window size must be chosen. It also allows the user to choose from a variety of different smoothing options and to choose which frequencies are not desired (slicing). An example output of the Fourier amplitude spectra and HVSR curve generated from *Grilla* can be seen in Figure(1.2). *hvsrpy* is an open-source Python package developed for HVSR processing (Vantassel 2020) and was the primary software used for interpretation of HVSR curves. It has been extensively tested against industry standard programs for HVSR analysis and has many advantages not found within traditional geophysical analysis programs. First, its free availability combined with clear documentation and high code quality allow for a very shallow learning curve, even for users with limited Python experience. *hvsrpy* allows for many more user options and features compared to *Grilla*, some of which are not currently available in any other commercial or open-source software

(a list of these features can be found here). One of these uniquely available features is the automatic checking of the SESAME fundamental site frequency (f_0) reliability and clarity conditions which proved extremely valuable for increasing the efficiency of workflow and confidence of reliable results. Examples of *hvsrpy* figure and console outputs can be seen in Figures(2.2 & 2.3), where Figure(2.2) represents a very clear and reliable fundamental site frequency peak, satisfying all six of the reliability conditions. Figure(2.3) represents poor HVSR data with no clear peak, only satisfying two out of six reliability conditions.

(a)   **(b)**
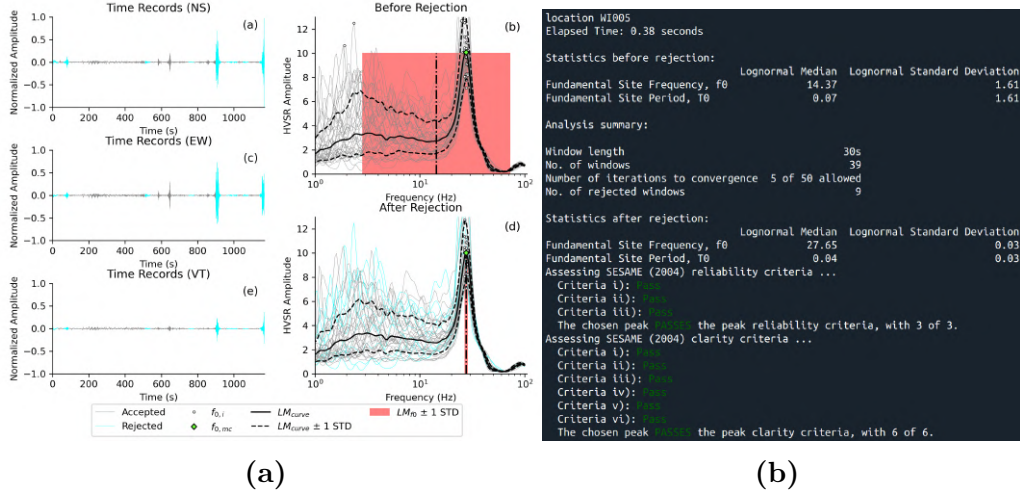
Figure 2.2 Example of *hvsrpy* figure (a) and console (b) output for a reliable HVSR curve and fundamental site frequency (f_0) peak.
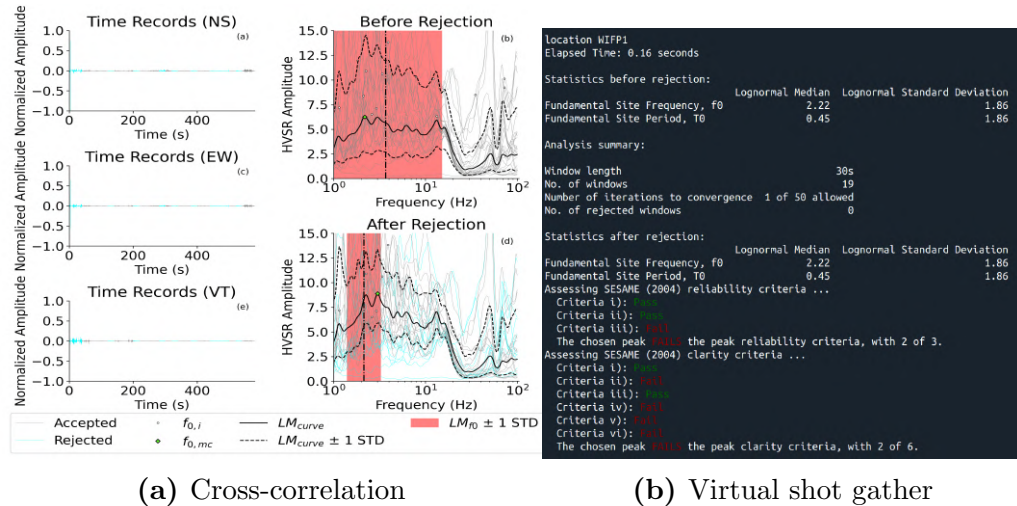
(a) Cross-correlation   **(b)** Virtual shot gather

Figure 2.3 Example of *hvsrpy* Figure (a) and console (b) output for an unreliable HVSR curve and fundamental site frequency (f_0) peak.

2.3   Shear-Wave Velocity Calculation

2.3.1   Multi-channel Analysis of Surface Wave Method (MASW)

The MASW method was first developed as a non-invasive and more economical alternative to shear wave refraction, down-hole and cross-hole surveys for the purpose of determining information on the elastic properties of near-surface materials (Park 1999). The MASW method uses lower frequency surface waves (1-30 Hz) while focusing on a shallow investigation depth range (on the order of a few 10^0-10^1 metres). Using this method, the ground roll from a single shot gather produces a highly accurate dispersion curve which can then be inverted to produce a shear wave velocity profile of the shallow subsurface with high confidence (Park 1999; Xia 1999; Park 2007). The main advantage with the MASW method comes from its ability to utilize the complex and varied nature of the entire seismic wavefield. The dispersion properties of all types of seismic waves are visualised through the transformed energy distribution which is generated from the wavefield-transformation of the multi-channel record (Park 2007; Park 1999). In the energy distribution image, the dispersion property of interest (such as the fundamental mode) can be obtained from easily identifiable patterns. Unwanted scattered and reflected waves can usually be removed from the energy distribution during the transformation (Park 2007). The 1D MASW method can be broken down into three main steps:

1. Acquire multi-channel field records (shot gather).

2. Extract dispersion curves.

3. Invert dispersion curves to obtain 1D shear wave velocity profile.

2.3.2   MASW acquisition and analysis

For MASW surveys using a multi-channel seismometer, a simple linear array with constant spacing between each channel (geophone) is generally assumed. Optimal field parameters for an MASW survey have been outlined by (Park 2002) and will serve as the basis for the survey geometry used in this research. Water well data was available for the MASW data collection site, indicating the soil thickness to be around 5m. Thus for an depth interest less than 10m, it was decided that a linear array 20m in length with

a 1m seismometer (geophone) spacing would provide more than enough information for an accurate characterisation of the soil layer. Recalling Section(2.1), a multi-channel seismometer was not available and only two three-component seismometers were used for this study. To overcome this issue, the construction of a virtual shot gather is required, resulting in active source generation for each seismometer spacing. Figure(2.4) represents the survey geometry used, where the red boxes labelled T1 and T2 represent two seismometers, and the blue circle labelled S represents the active source which was a 10kg sledgehammer and metal plate. Starting from the top of Figure(2.4), the survey is set up linearly with T1 being a distance $x_1 = 3$m from the source and T2 being $x_1 = 1$m away from T1. The seismometers would then start recording and an active source would be generated (sledgehammer hit). After the recordings stop, T2 would then be moved another $x_2=1$m away from T1, resulting in a separation of $2x_2=2$m between the two seismometers. At this point, new recordings would start and an active source would once again be generated. Once the recordings stop, T2 would be moved another $x_2=1$m away from T1, resulting in a separation of $3x_2=3$m between the seismometers. This procedure was carried out until the seismometers reached a final spacing of $18x_2=18$m (20m wasn't able to be reached due to lack of sunlight).
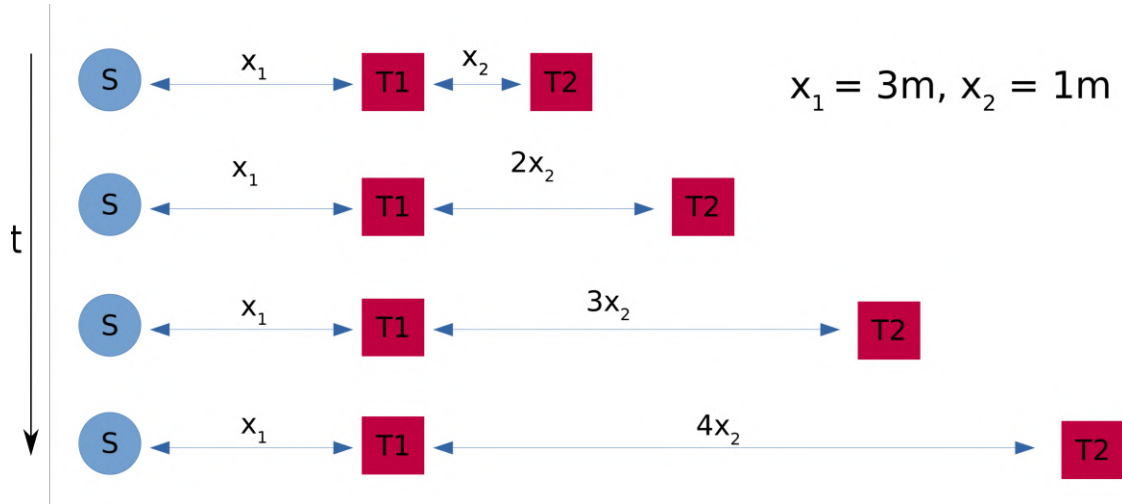
Figure 2.4 Schematic of survey layout. T1 and T2 represent the stationary and moving seismometer respectively. S represents the location of the active source (sledgehammer). x_1 represents the distance from the stationary seismometer and the source. x_2 represents the spatial increment of separation between the seismometers. The t and arrow on the left-hand side represent the fact that each survey layout was performed one at a time, starting with a seismometer separation of x_2 and continuing until $18x_2$.

In order to relate the seismic recordings from each survey geometry and reconstruct

the generated surface wave pulse, a cross-correlation technique was used. Also known as a sliding dot product, cross-correlation tracks the relative displacements of two or more sets of time-series data (Bourke 1996). It can be thought of as the measure of the similarity between two or more time-series data. Figure(2.5a) shows the time signal reconstructed after cross-correlation between seismometer recordings separated by $3x_2=3m$. Once cross-correlations were computed for each survey geometry, they were stacked to create a virtual shot gather as seen in Figure(2.5b).

(a) Cross-correlation   **(b)** Virtual shot gather
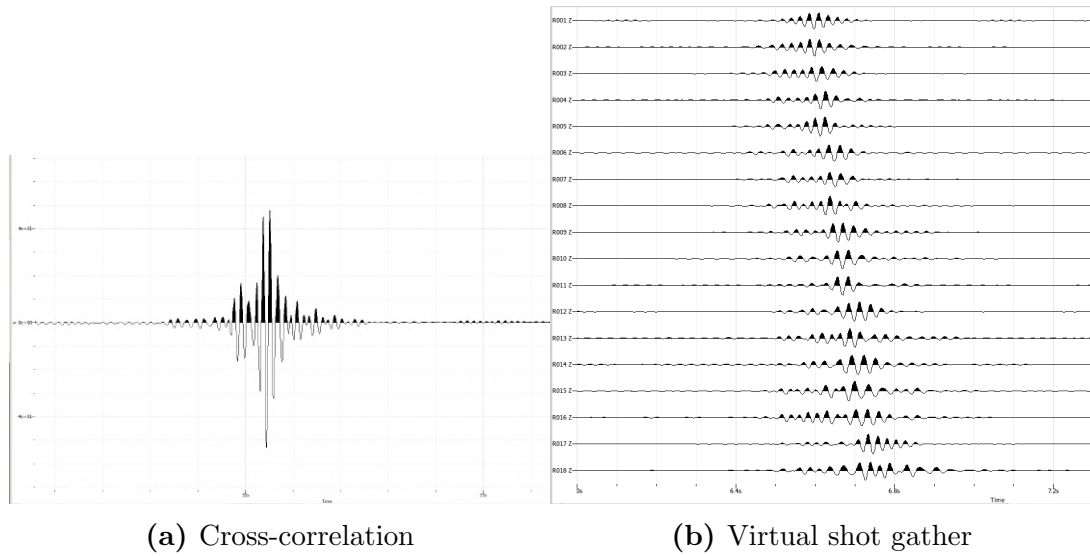
Figure 2.5 (a) Time series of cross-correlated recordings from seismometers separated by $3x_2=3m$. (b) Virtual shot gather obtained from stacking each cross-correlation.

Now that we have completed step 1 of the MASW method, the next step is the extraction of dispersion curves. Many software designed for geophysical research can automatically compute dispersion curves directly from a shot gather. Figure(2.6) shows the resultant dispersion curve of surface waves generated from the shot gather shown in Figure(2.5b). Frequency is represented along the y-axis and the phase velocity of surface waves is represented along the x-axis. The pattern representing the fundamental mode is clearly seen and highlighted by the dark blue regions of the curve which were manually picked/traced by the red dots.
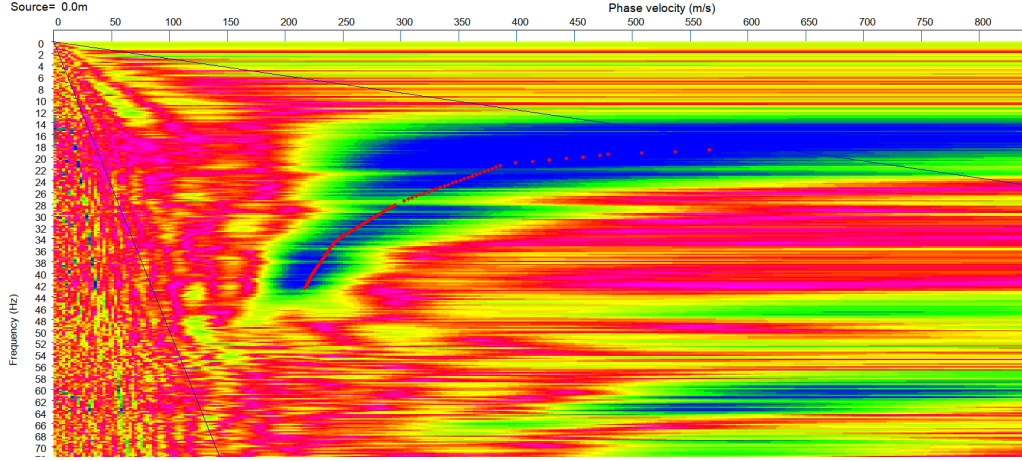
Figure 2.6 Dispersion curve of surface wave phase velocity generated from virtual shot gather in Figure(2.5b). Red dots represent manual picks along the fundamental mode.

Moving on to the final step, the manual picks along the dispersion curve are then inverted to show the 1D shear wave velocity profile as seen in Figure(2.7). Again, the inversion of the dispersion curve is automatically calculated by many geophysical software programs.
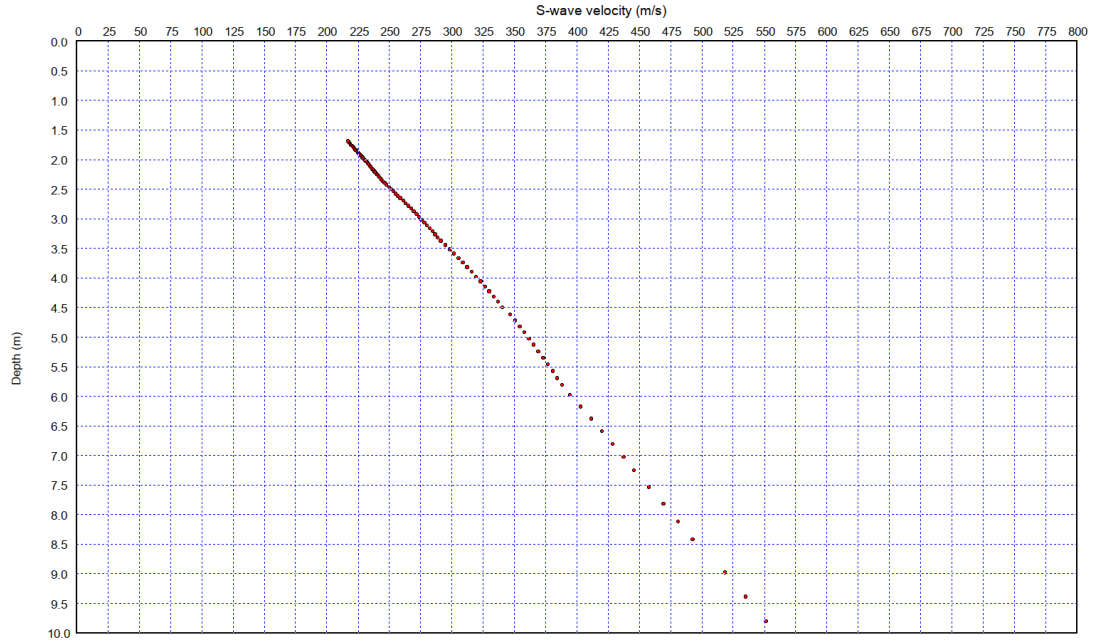
Figure 2.7 1D shear wave velocity profile obtained from the inversion of the dispersion curve seen in Figure(2.6)

Chapter 3

Results and Discussion

3.1 Shear Wave Velocity

Eq(1.1) can be rearranged to the following expression:

$$h = \frac{V_s}{4f_0} \tag{3.1}$$

where h is the soil thickness (depth to bedrock), f_0 is the fundamental site frequency and V_s is the average shear wave velocity of the soil layer. Now that a shear wave velocity profile has been obtained, an average value must be determined. The 1D shear wave velocity profile shown in Figure(3.1) depicts a clear relationship between shear wave velocity and depth. Approximating a linear relationship would dictate there is a 50m/s increase in the shear wave velocity for every 1m increase in depth. Assuming this rate of change, a simple linear function can be constructed to estimate shear wave velocity as a function of depth. Taking the mean of the function from the surface to the depth to bedrock allows one to obtain the average shear wave velocity of the soil for a given soil thickness or depth to bedrock. If we apply this for soil thicknesses of 1m and 10m, then the average shear wave velocities obtained are $V_s = 150m/s$ and $V_s = 375m/s$ respectively. This corresponds to a difference of over 200m/s which emphasises the fact that even if the soil composition is the same, varying the soil thickness on the order of only a few metres results in significantly different values for the average shear wave velocity of the soil. Thus, using an average shear wave velocity for all sites on Wolfe Island is an inadequate approach to obtain accurate estimates for soil thickness.
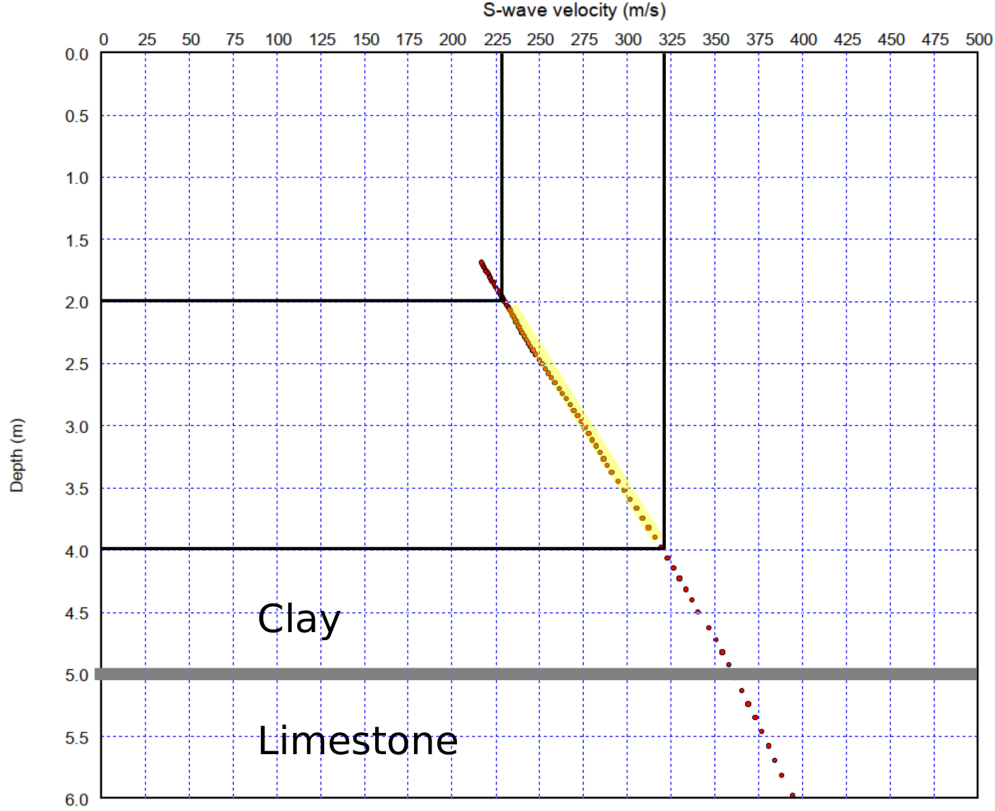
Figure 3.1 1D shear wave velocity profile up to 6m in depth. Horizontal line at a depth of 5m represents the approximate boundary between limestone bedrock and clay soil layer, as per water well data.

There are a number of different approaches to this problem. One such approach is to simply omit the requirement of an average shear wave velocity of soil and collect a sufficient amount of fundamental site frequencies near known values of soil thickness such that relation only between the fundamental site frequency and soil thickness can be developed. This approach was not feasible due to the limited amount of data in close proximity to water wells, not allowing for a reliable relation to be calculated. Another approach is to simply obtain shear wave velocity profiles at each new site, however this could not be done due to time constraints. The approach taken to solve this issue is to utilise the available water well data to refine the average shear wave velocity estimation at each site. The first step in this process is to create a model of the shear wave velocity of the soil as a function of depth. As seen in Figure(3.1), data above 2m in depth is not shown, as these depths did not clearly represent the fundamental mode pattern seen in Figure(2.6). Furthermore, water well data only a few tens of metres away suggest that the soil thickness at this site is approximately $h=5$m. This results in a depth range between 2 and 4 metres which accurately represents the shear wave velocity of the compact clay

16

layer. The slopes from a few different shear wave velocity profiles derived from slightly different manual picks of the dispersion curve can be averaged to obtain a relationship which calculates shear wave velocity as a function of depth. The equation can be expressed as:

$$V_s(z) = mz + V_{sg} \tag{3.2}$$

where V_s is the shear wave velocity in metres per second, z is depth in metres, V_{sg} is the shear wave velocity of the soil near the surface with a value of 125m/s and m represents the rate of change between the shear wave velocity and depth with a value of $50\frac{m/s}{m}$. The accuracy of this function can be constrained using other site-specific geological information. Analysis of the water well data at this site dictates the depth to bedrock to be located at precisely h=5.2m. Moreover, an average of three HVSR curves at the site suggests a fundamental site frequency of f_0=11.8Hz. Using this information in Eq(3.1) generates an expected value of the average shear wave velocity of the soil layer to be 245m/s. Now, using Eq(3.2) for a soil thickness of 5.2m, the mean value is determined to be 250m/s, which is in close agreement with the expected average shear wave velocity obtained from using Eq(3.1). Thus we can conclude that this linear model is a *reasonable approximation* to the physical values. Additionally, since the soil thickness on Wolfe Island ranges from 0-10m, the average shear wave velocity for the soil from a site with a soil thickness of 5m serves as a fair assumption for the average shear wave velocity for the soil layer of the entire island. This can be taken one step further to which a lower and upper limit of the average shear wave velocity can be estimated. For the lower limit, the average value of Eq(3.2) for $h = 0$m, results in V_s= 125m/s. Likewise, using the maximal depth to bedrock of $h = 10$m, the average shear wave velocity is calculated to be 375m/s.

This simple model assumes that the shear wave velocity very close to the surface and at the bedrock/soil interface is represented by the same linear relationship. However, it is widely known that there usually exists at least four distinct layers between the surface and intact/solid bedrock: (i) a thin layer of loose soil followed by (ii) a more compact layer of subsoil, followed by (iii) a thin layer of fractured or weathered bedrock and then finally (iv) intact/solid bedrock. Therefore, we can modify this function to allow for variability in the loose soil and weathered bedrock layers. The modified function can be expressed as:

$$
V_s(z) = \begin{cases}
m_s z + V_{ss}, & \text{for } z < h_s \\
m z + V_{sg}, & \text{for } h_s < z < h_b \\
m_b z + V_{sb}, & \text{for } h_b < z
\end{cases}
\tag{3.3}
$$

where h_s and h_b represent the depth to loose/stiff soil interface and stiff soil/weathered bedrock interface respectively. m_s and m_b represent the different rates of change between the shear wave velocity and depth for the loose soil and weathered bedrock layers respectively. V_{ss} and V_{sb} are constants which represent the theoretical shear wave velocity at the surface for loose soil and weathered bedrock respectively. The remaining variables z, m and V_{sg} represent the same variables as for Eq(3.2). Importantly, the modified linear functions for the loose soil and weathered bedrock layer are on-top of step function changes in the shear wave velocity. For example, Figure(3.2b) represents the use of Eq(3.3) at a site where the soil thickness is known to be 5.8m. The water well data also indicates fractured bedrock between 4.9-5.8m in depth. While there is no distinction between compact and loose soil layers, the thickness of the loose soil layer was assumed to be 0.4m. This assumption was made on the basis that the soil is currently being used for a young tree plantation and thus the top layer of soil must have been tilled within the last couple years.

(a) Vs profile as described by Eq(3.2)   **(b)** Vs profile as described by Eq(3.3)
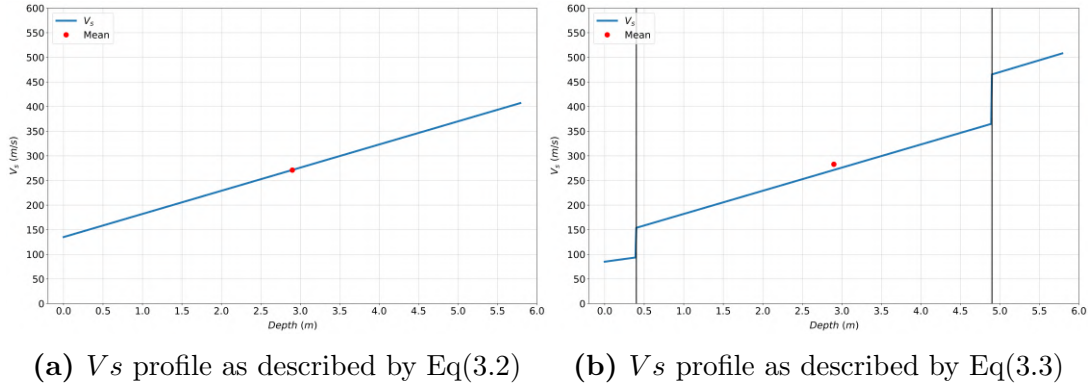
Figure 3.2 Calculated shear wave velocity profiles using different models for a site with soil thickness of 5.8m. Mean values are represented by the red dot. Vertical black line at depth=0.4m in (b) represents boundary between stiff soil and loose soil. Vertical black line at depth=4.9m in (b) represents boundary between stiff soil and fractured bedrock. Values for the parameters of both models can be found in Table(3.1)

m (1/s)	m_s (1/s)	m_b (1/s)	V_{sg} (m/s)	V_{ss} (m/s)	V_{sb} (m/s)	h_s (m)	h_b (m)	$h(m)$
50	50	25	125	85	225	0.4	4.9	5.8

Table 3.1: Table of parameters used in Eq(3.2) and Eq(3.3) to generated V_s profiles seen in Figure(3.3)

Evidently, the addition of the variable layers of loose soil and weathered bedrock leaves room for a lot of speculation and assumptions. These assumptions are primarily guided by information provided by water well data which can lack detailed information, especially for older data. Conversations with land-owners and visual inspection gives site-specific knowledge of previous and current land-use which played a key role in the determination of loose soil layer parameters. For each site, the soil thickness from the nearest water well was used in both Eq(3.2) and Eq(3.3) to estimate the average shear wave velocity of the soil. A combination of these values, along with site-specific geological information were used to determine the average shear wave velocity of the soil. For the majority of cases, estimates from both models only varied by 5m/s at most, resulting in relatively minute changes in the estimation of soil thickness.

3.2   Soil Thickness Estimates

A total of 55 individual recordings were collected over the course of five days and approximately 20-25 hours of data collection. 12 recordings were rejected as their HVSR curves did not show a clear and reliable fundamental site frequency. There are a number of different plausible reasons for the cause of poor HVSR curves that are discussed in Chapter(5.2). This leaves 43 remaining recordings that showed clearly identifiable fundamental site frequency peaks in their HVSR curve. For each of the remaining recordings, four separate soil thickness estimates were computed from four separate average shear wave velocity values. Three of the average shear wave velocities remained constant among all the recordings, representing the computed mean values of the function described by Eq(3.2). Two of these values were computed using h=0m and h=10m which represents lower and upper limits of the expected average shear wave velocity range. The third constant shear wave velocity was calculated using h=5m which represents the average shear wave velocity of the soil expected for the whole island. These values were computed to be 125m/s, 375m/s and 250m/s for the lower limit, upper limit and average shear wave

velocity respectively. Finally, for each recording a unique average shear wave velocity of the soil was computed using the soil thickness of the nearest water well available.

These estimations of soil thickness are shown in Figure(3.3), where the circles correspond to water well data and the diamonds represent the estimations from this study. A limited amount of information can be drawn from a non-interactive version of the map, however, it is clear to see that no significant anomalies exist between the soil thickness from the water well data and the estimations of soil thickness made in this study. Furthermore, a few sites very close to water well data show the same or a very close colour pattern, signifying the estimations of soil thickness are within a couple metres of the well data at most. For a more detailed view of the map, shapefiles for the data can found alongside this publication.
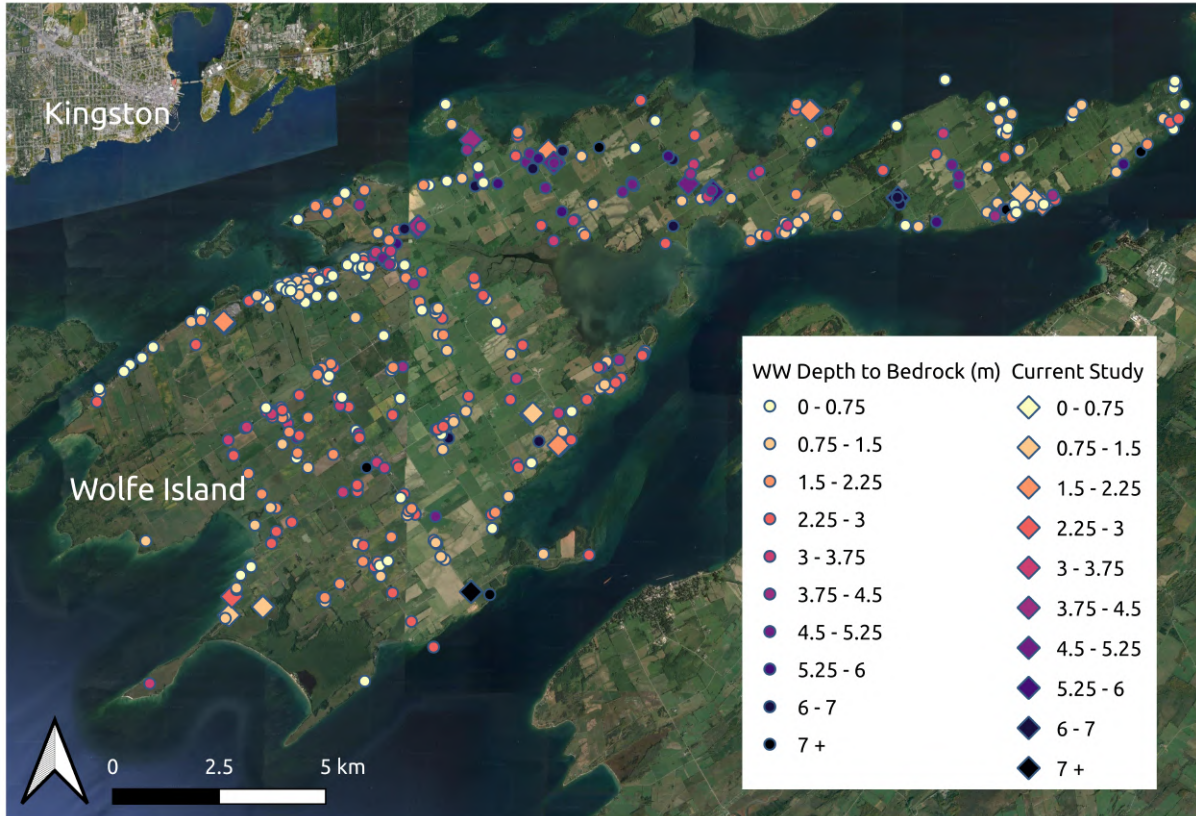
Figure 3.3 Map of Wolfe Island with depth to bedrock/soil thickness values from water well data (circles) and estimated values from the HVSR method (Diamonds).

A more rigorous comparison between the estimates of soil thickness and water well data can be done by only using data collected in close proximity to a water well. Here, close proximity was decided to be within 500m of the collected data. Although significant variations in soil thickness can occur in only a few tens of metres, water well data on the

island suggests that in most cases soil thickness only varies by a couple metres (at most) over a distance of a few hundred metres. Also, a smaller range would only allow for the analysis of a few sites since most of the data was not collected in very close proximity (less than 100m) of a water well. Clearly, the closer a site is to a water well, the less likely of a significant change in soil thickness, resulting in the sites of closer proximity holding more significance in their results. Nevertheless, for a site within this proximity, all the fundamental site frequency estimations and measured distances to the nearest water well would be averaged. Figure(3.4) shows estimates for soil thickness/depth to bedrock on the y-axis with the corresponding distance to the nearest water well on the x-axis. The black crosses represent soil thickness as indicated from the water well data, while cyan dots represent estimates of soil thickness using the average shear wave velocity for the islands soil layer (V_s=250m/s). The error bars represent soil thickness estimates using the lower and upper limits of the average shear wave velocity (lower = 125m/s, upper = 375m/s). The magenta dots represent the estimated soil thickness using a unique shear wave velocity as determined by the methods outlined in Section(3.1). It was found that using V_s=250m/s for all sites on the island resulted in an average difference between the estimated and measured (from water wells) soil thickness to be 1.06m. Conversely, using a unique shear wave velocity of the soil layer for each site resulted in an average difference between the estimated and measured (from water wells) soil thickness to be only 0.43m. A few key results can be taken from this with the most obvious being the use of a unique average shear wave velocity of the soil layer resulted in estimates of soil thickness which were significantly closer to water well data than did the island-wide average shear wave velocity. The inaccuracy of the island-wide average shear wave velocity were emphasised for relatively shallow and deep soil thicknesses. More specifically, estimates of soil thickness were generally overestimated for sites where the water well indicates a soil thickness less than 5m. Likewise, for sites where the water well records indicate a soil thickness more than 5m, estimates of soil thickness were generally underestimated. Finally, the measured soil thickness from water wells all fell within the range of soil thicknesses as calculated by the lower and upper limits of the average shear wave velocity.
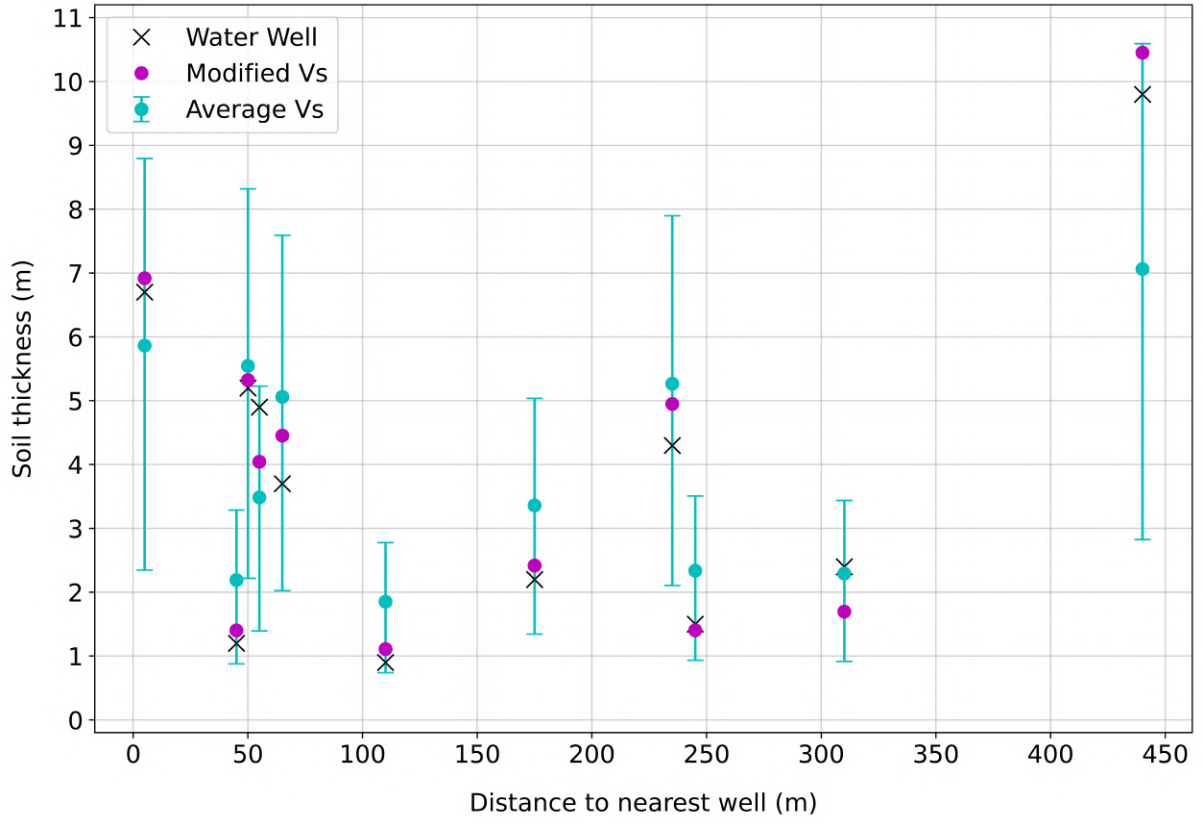
Figure 3.4 Estimations for depth-to-bedrock/soil thickness for sites within 500m of the nearest nearest water well using an island-wide average V_s (cyan dot) and site-specific unique average V_s (magenta dot). Error bar range correspond to estimates of soil thickness made using lower (125m/s) and upper limits (375m/s) of average V_s. Soil thickness values from water well data represented by black crosses (x).

Chapter 4

Conclusions

Site characterisation on Wolfe Island, Ontario has been almost exclusively done via traditional methods of drilling. This makes the already expensive method extra costly due to the extended vehicle travel time to and from the island which can only be done by ferry. Site-specific geological parameters such as depth to bedrock/soil thickness (h) is of significant interest to many land-owners on the island. This information plays a critical component in planning the ideal location of construction operations such as a house, barn or shed. Since most of the land on Wolfe Island is used for agricultural purposes, depth to bedrock also plays a crucial role to ensure optimal crop yield. The horizontal to vertical spectral ratio (HVSR) method serves as a non-invasive, fast and inexpensive method to determine the fundamental site frequency (f_0) which can then be used to estimate of the depth to bedrock/soil thickness. The interest of many landowners suggests the usefulness and potential economic viability of this method as a cheaper alternative to drilling when an exact value for the soil thickness is not required. In total, 55 separate microtremor recordings over the course of approximately 20-25 hours of solitary field work verify the impressive speed at which data can be acquired. Of these 55 recordings, 12 were not used as they did not provide a clear value of the fundamental site frequency. It was found that the use of a singular average shear wave velocity (V_s) to represent the soil layer of the entire island resulted in relatively inaccurate estimates of the soil thickness. This was especially emphasised at sites where water well data suggests a relatively shallow ($\sim$ 1-2m) or deep ($\sim$ 7-10m) soil thickness compared to the island average ($\sim$3-6m). However, it was found that the use of a unique average shear wave velocity of the soil layer guided by water well data for each site resulted in an increased robustness of soil thickness estimates. In summary, 43 microtremor recordings on the island resulted in clear fundamental site

frequencies which were used to estimate soil thickness or depth-to-bedrock. Both of these data-sets can be found alongside this study.

4.1 Limitations & Future work

The primary limitation of this study was the lack of a sufficient amount of data collected near known soil thicknesses. Time was the major limiting factor, as it required a great deal of logistical effort to get in contact with land-owners. This allowed for a limited selection of sites based on available water well data which resulted in only going to sites where permission was granted. This led to a limited ability to properly compare estimated and measured (from water wells) soil thicknesses. Moreover, a straightforward statistical analysis of the data with any real significance was not feasible. Therefore, the primary objective for future work related to this study would be to collect a substantially larger amount of data, especially in close proximity (less than 50m) to available water well data. Given enough data, it would also allow for the development of a relationship only between the fundamental site frequency and soil thickness, omitting the dependence on the average shear wave velocity of the soil layer for estimates of soil thickness (Seht 1999; Yilar 2017; Tian 2019). Nevertheless, further utilisation of the MASW method at a variety of locations on the island would be pivotal to refine and increase the robustness and accuracy of the shear wave velocity model of the soil layer. Furthermore, a detailed mapping of the bedrock topography would conceivably be possible, given a sufficiently dense and evenly spaced array of measurements (which would have many advantages to geologists). Much of the suggested future work could be obtained at a lower cost and reduced acquisition time with improved instruments. For example, the use of two seismometers only allows for about two recordings in 30 minutes at maximal efficiency. However, the use of fibre optic cables would allow for a dramatic increase in spatial range and resolution, at the cost of increased initial set-up time. In fact, fibre optics have already been applied in urban settings for the purpose of site characterisation. It was found that HVSR and Rayleigh wave dispersion curves could be generated and jointly inverted to obtain a model of shallow seismic velocities and soil thickness (Spica 2020). The use of fibre optics would be especially valuable in urban settings that have pre-existing fibre optic infrastructure in place, minimising time spent acquiring data. The unprecedented growth of fibre optic infrastructure in the recent decades have resulted in

thousands of kilometres of *dark* (unused) cables which are already in place and ready to be used for seismological purposes.

25

References

K. Aki. Space and Time Spectra of Stationary Stochastic Waves, with Special Reference to Microtremors. *Bulletin of the Earthquake Research Institute*, 35:415–456, **1957**. http://oceanrep.geomar.de/43280/1/Aki.pdf.

S. Assefa, C. McCann, and J. Sothcott. Velocities of Compressional and Shear Waves in Limestones. *Geophysical Prospecting*, 51(1):1–13, **2003**. https://onlinelibrary.wiley.com/doi/abs/10.1046/j.1365-2478.2003.00349.x.

P.-Y. Bard. Microtremor Measurements: A Tool for Site Effect Estimation? volume 3, pages 1251–1279, 12 **1998**. https://www.researchgate.net/publication/235623097_Microtremor_measurements_A_tool_for_site_effect_estimation.

V. Bennett, K. Bowman, and S. Wright. Optimum Field Parameters of an MASW Survey. Technical report, Kansas Geological Survey and Terra Corporation, Tokyo.

P. Bourke. Cross Correlation. **1996**. https://www.researchgate.net/profile/Paul-Bourke-2/publication/245817141_Cross_correlation_autocorrelation_2d_pattern_identification/links/0046352c36f114ecbf000000/Cross-correlation-autocorrelation-2d-pattern-identification.pdf.

S. Braganza, G. M. Atkinson, H. Ghofrani, B. Hassani, L. Chouinard, P. Rosset, D. Motazedian, and J. Hunter. Modeling Site Amplification in Eastern Canada on a Regional Scale. *Seismological Research Letters*, 87(4):1008–1021, 06 **2016**. ISSN 0895-0695. https://doi.org/10.1785/0220160009.

G. Giannaraki, I. Kassaras, and Z. Roumelioti. Deterministic Seismic Risk Assessment in the City of Aigion (W. Corinth Gulf, Greece) and Juxtaposition with Real Damage due to the 1995 Mw6.4 Earthquake. *Bulletin of Earthquake Engineering*, 17:603–634, **2019**. https://doi.org/10.1007/s10518-018-0464-z.

M. Ibs-von Seht and J. Wohlenberg. Microtremor Measurements used to Map Thickness of Soft Sediments. *Bulletin of the Seismological Society of America*, 89(1):250–259, 02 **1999**. ISSN 0037-1106. https://doi.org/10.1785/BSSA0890010250.

J. John W. Lane, E. A. White, G. V. Steele, and J. C. Cannia. Estimation of Bedrock Depth Using the Horizontal-to-Vertical (H/V) Ambient-Noise Seismic Method. *Symposium on the Application of Geophysics to Engineering and Environmental Problems 2008*, pages 490–502, **2008**. https://library.seg.org/doi/abs/10.4133/1.2963289.

J.-S. L'Heureux and M. Long. Relationship between Shear-Wave Velocity and Geotechnical Parameters for Norwegian Clays. *Journal of Geotechnical and Geoenvironmental Engineering*, 143(6):04017013, **2017**. https://doi.org/10.1061/(ASCE)GT.1943-5606.0001645.

M. Mucciarelli. Ambient Noise Measurements following the 2011 Christchurch Earthquake: Relationships with Previous Microzonation Studies, Liquefaction, and Nonlinearity. *Seismological Research Letters*, 82(6):919–926, 11 **2011)**. ISSN 0895-0695. https://doi.org/10.1785/gssrl.82.6.919.

M. Mucciarelli and M. Gallipoli. A Critical Review of 10 years of Microtremor HVSR Technique. *Bulletin of Theoretical and Applied Geophysics*, 42:255–266, 09 **2001**. https://www.researchgate.net/publication/279895512_A_critical_review_of_10_years_of_microtremor_HVSR_technique.

Y. Nakamura. Dynamic Characteristics Estimation of Subsurface using Microtremor on the Ground Surface. *Quarterly Report of Railway Technical Research*, pages 25–33, **1989**. ISSN 30(1). https://doi.org/10.1186/s13634-021-00765-z.

Ontario Ministry of the Environment, Conservation and Parks. Ontario well records. Miscellaneous Release, **1899 - 2021**. https://data.ontario.ca/dataset/well-records.

F. Panzera, G. Romagnoli, G. Tortorici, S. D'Amico, M. Rizza, and S. Catalano. Integrated use of Ambient Vibrations and Geological Methods for Seismic Microzonation. *Journal of Applied Geophysics*, 170:103820, **2019**. ISSN 0926-9851. https://doi.org/10.1016/j.jappgeo.2019.103820.

C. B. Park, R. D. Miller, and J. Xia. Multichannel Analysis of Surface Waves. *GEOPHYSICS*, 64(3):800–808, **1999**. https://doi.org/10.1190/1.1444590.

C. B. Park, R. D. Miller, J. Xia, and J. Ivanov. Multichannel Analysis of Surface Waves (masw) — Active and Passive Methods. *The Leading Edge*, 26(1):60–64, **2007**. http://dx.doi.org/10.1190/1.2431832.

S. Parolai. Investigation of site response in urban areas by using earthquake data and seismic noise. **2012**. https://doi.org/10.2312/GFZ.NMSOP-2_ch14.

A. Rigo, E. Sokos, V. Lefils, and P. Briole. Seasonal Variations in Amplitudes and Resonance Frequencies of the HVSR Amplification Peaks Linked to Groundwater. *Geophysical Journal International*, (1):1–13, 03 **2021**. ISSN 0956-540X. https://doi.org/10.1093/gji/ggab086.

SESAME. Guidelines for the Implementation of the H/V Spectral Ratio Technique on Ambient Vibrations Measurements, Processing and Interpretation. 6, **2005**. SESAME European Research Project http://sesame.geopsy.org/Papers/HV_User_Guidelines.pdf.

Z. J. Spica, M. Perton, E. R. Martin, G. C. Beroza, and B. Biondi. Urban Seismic Site Characterization by Fiber-Optic Seismology. *Journal of Geophysical Research: Solid Earth*, 125(3):e2019JB018656, **2020**. https://agupubs.onlinelibrary.wiley.com/doi/abs/10.1029/2019JB018656.

The Ontario Geological Survey. Surficial Geology of Southern Ontario. Miscellaneous Release–Data 128-REV, **2004**. http://geo1.scholarsportal.info/#r/details/_uri@=213781795.

B. Tian, Y. Du, Z. You, and R. Zhang. Measuring the Sediment Thickness in Urban Areas using Revised H/V Spectral Ratio Method. *Engineering Geology*, 260:105223, **2019**. ISSN 0013-7952. https://doi.org/10.1016/j.enggeo.2019.105223.

J. Vantassel. jpvantassel/hvsrpy. http://doi.org/10.5281/zenodo.3666956, **2020**.

J. Xia, R. D. Miller, and C. B. Park. Estimation of Near-Surface Shear-Wave Velocity by Inversion of Rayleigh Waves. *GEOPHYSICS*, 64(3):691–700, **1999**. `https://doi.org/10.1190/1.1444578`.

W. L. Xu, Rong. The Horizontal-to-Vertical Spectral Ratio and its Applications. *EURASIP Journal on Advances in Signal Processing*, **2021**. `https://doi.org/10.1186/s13634-021-00765-z`.

N. Yilar, L. G. Baise, and J. E. Ebel. Using (H/V) Measurements to Determine Depth to Bedrock and V_{s30} in Boston, Massachusetts. *Engineering Geology*, 217, **2017**. `https://doi.org/10.1016/j.enggeo.2016.12.002`.

Chapter 5

Appendix

5.1 Software Comparison

As described in the methods, two separate software packages were used to calculate fundamental site frequency values (f_0). In Figure(5.1), the calculate values for the fundamental site frequencies have been plotted against the different site locations. Evidently, the two software produce very similar values, with a few locations having a difference of a few hertz. The average difference between the fundamental site frequency calculate by the two software is approximately 0.25Hz. This comparison provides verification that both software produce accurate and reproducible HVSR curves.
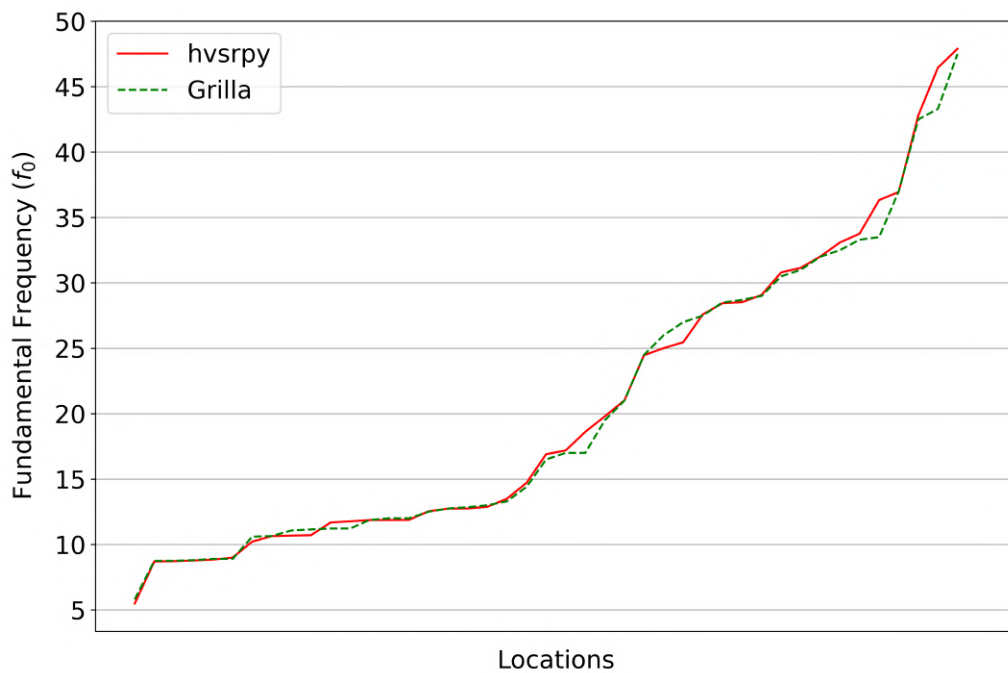
Figure 5.1 Comparison between fundamental site frequency (f_0) as calculated by *Grilla* and *hvsrpy*.

5.2 Anomalies & Sources of Error

There are a number of possible origins for unclear peaks seen in HVSR curves (SESAME 2004). Some examples include: meteorological perturbations, bad soil-sensor coupling, low frequency artificial ambient vibration sources, inadequate smoothing parameters, high wind speeds and underground lateral variation (faults and slopes). For this study, most of sources for unclear fundamental site frequencies can be categorised into two main causes: resonators and grass/vegetation.

5.2.1 Resonators

Perhaps the most valuable source of an unclear fundamental site frequency peak is caused by a resonator. In this case a resonator is any structure, especially buried underground, that will include frequencies in the HVSR which are unrelated to the fundamental site frequency. The SESAME guidelines advise the avoidance of measurements taken near buildings, trees, etc., in the case of strong winds as it can induce low frequencies in the curves which will alter the results (SESAME 2004). Furthermore, measuring above underground structures are also suggested to be avoided as they induce frequencies that will alter the results (SESAME 2004). In this study, measurements taken within a metre of light posts and water wells showed clear secondary peaks of higher frequency compared to the fundamental site frequency. More interestingly, at one site, data was collect on-top of and around a buried cement cistern. The top of the cistern is about 0.6m from the surface and has dimensions similar to that of a small car. Figure(5.2) depicts three separate mean HVSR curves measured at various distances away from the cistern. For the two measurement taken just metres away from a cistern, a clear secondary peak around 30-40Hz is seen. It is important to note that the fundamental site frequency of about 20Hz has an amplitude larger than the secondary peak by at least a factor of two. However, for the measurement right on-top of the cistern, both peaks have nearly the same amplitude. This is likely due to the increased amplification of the cistern's natural frequency from being directly on-top of it. Therefore, although measurement near and on-top of structures can have a significant influence on reading the fundamental site frequency from the HVSR curve, it can give valuable insight into the natural frequencies of subsurface structures. This can have major benefits in the realm of geophysical prospecting for studies of the dynamical behaviour of buildings and other structures (Mucciarelli

2001).
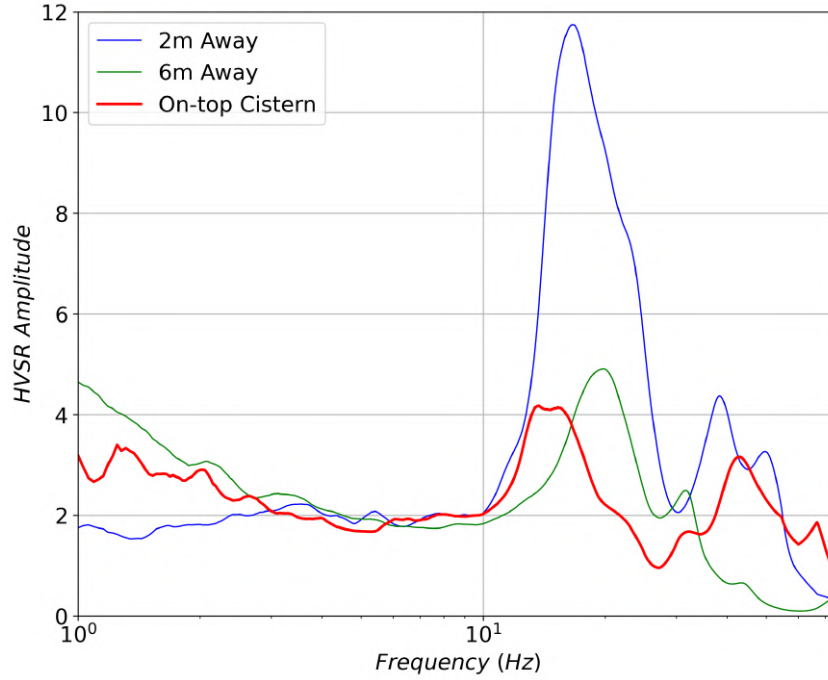
Figure 5.2 A variety of mean HVSR curves with varying distances away from a buried cement cistern.

5.2.2   Grass & Vegetation

The effect of grass and vegetation such as trees have been documented as known sources of creating an unclear HVSR fundamental site frequency peak (SESAME 2004). A few measurements taken within a forest resulted in poorly defined HVSR curves due to the effect the large roots have on microtremors in the subsurface. More prevalent was the issue of measuring around or within long grass. As many of the measurements were not taken in open farm fields, long grassy yards were hardly uncommon. Most of the time, patches of dead or short grass were found where measurements would then be taken. However, in a few cases grasses of ∼0.5m had to be dealt with. Ideally, the grass can simply be removed but long grass was proven to be very difficult to remove. Figure(5.3) shows an example of the difference tall and short grass can have in the HVSR curve from the same site. It is evident that the long grass reduced the amplitude of the HVSR curve across all frequencies, and especially in the lower frequency range.
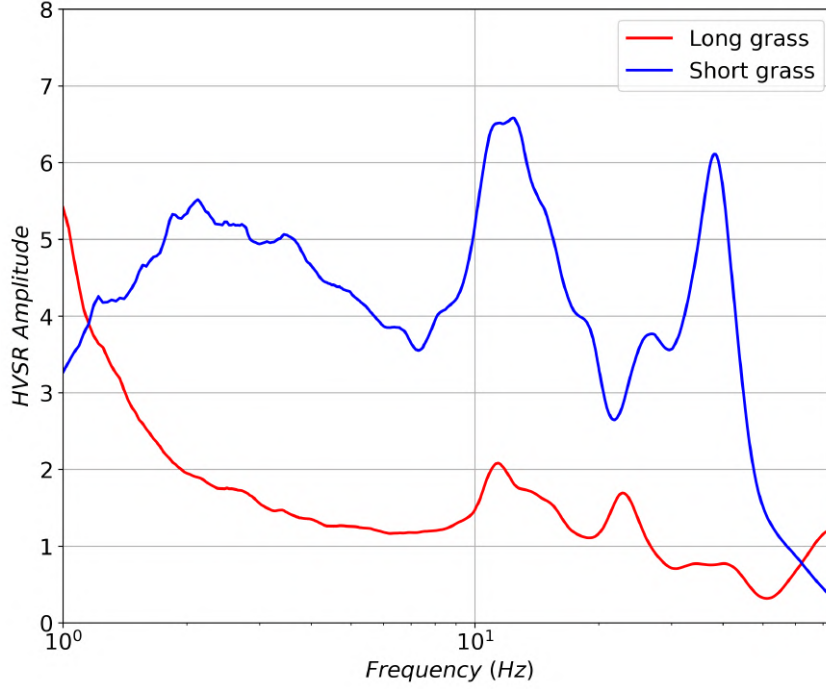
Figure 5.3 Mean HVSR curves showing the difference in amplitude when measurements were taken on short and long grass.

5.3   SESAME Conditions of Reliability

Below find a detailed list of the six conditions of reliability as outlined by SESAME:

Amplitude Conditions:

(i) there exists one frequency f^-, lying between $f_0/4$ and f_0, such that $A_0/A_{HVSR}(f^-) > 2$

(ii) there exists one frequency f^+, lying between f_0 and $4f_0$, such that $A_0/A_{HVSR}(f^+) > 2$

(iii) $A_0 > 2$

Stability Conditions:

(iv) the peak should appear at the same frequency (within a percentage $\pm$ 5%) on the HVSR curves corresponding to mean + and – one standard deviation.

(v) σ_f lower than a frequency dependent threshold $\epsilon(f)$

(vi) $\sigma_A(f_0)$ lower than a frequency dependent threshold $\Theta(f)$

where the parameters above represent:

- f = current frequency

- f_0 = HVSR peak frequency

- A_0 = HVSR peak amplitude at frequency f_0

- $A_{HVSR}(f)$ = HVSR curve amplitude at frequency f

- f^- = frequency between $f_0/4$ and f_0 for which $A_{H/V}(f^-) < A_0/2$

- f^+ = frequency between $f_0/$ and $4f_0$ for which $A_{H/V}(f^+) < A_0/2$

- $\sigma_A(f)$ = standard deviation of $A_{HVSR}(f)$, $\sigma_A(f)$ is factor by which the mean $A_{HVSR}(f)$ curve should be multiplied or divided.

- σ_f = standard deviation of HVSR peak frequency $(f_0\sigma_f)$

- $\epsilon(f_0)$ = threshold value for the stability condition $\sigma_f < \epsilon(f_0)$

- $\Theta(f_0)$ = threshold value for the stability condition $\sigma_A(f) < \Theta(f_0)$

5.4   Table of Values

Table(5.1) contains the most relevant values to this study. The latitude and longitude of each measurement is indicated, along with the fundamental site frequency (f_0) estimates from both *Grilla* and *hvsrpy* software (measured in Hz). V_s mod. represents the unique average shear wave velocity of the soil determined for each site (measured in m/s). h_{ave} represent the estimated soil thickness as calculated using the average sear wave velocity for the soil layer of the whole island (250m/s). h_{mod} represents the estimated soil thickness as calculated using the site-specific average shear wave velocity of the soil (V_s mod.). SC represents the amount of reliability conditions satisfied as outlined by SESAME (measured out of six). A more detailed table of values, including data on the rejected HVSR curves can be found alongside this report.

Latitude	Longitude	$hvsrpy$ f_0	$Grilla$ f_0	V_s mod.	h_{ave} (m)	h_{mod} (m)	RC
44.218973	-76.367018	19.8	19.5	290	3.16	3.66	6
44.219162	-76.366992	17.19	17	290	3.64	4.22	6
44.219782	-76.367333	16.9	16.5	290	3.7	4.29	5
44.220127	-76.367702	21.02	21	290	2.97	3.45	5
44.221237	-76.368525	32.02	32	290	1.95	2.26	4
44.221627	-76.368707	42.8	42.5	290	4.31	1.69	5
44.215156	-76.327415	11.87	12	240	5.27	5.05	4
44.230915	-76.291435	30.8	31	200	2.03	1.62	6
44.231005	-76.292003	27.59	27.5	200	2.27	1.81	6
44.211937	-76.223298	24.47	24.5	150	2.55	1.53	5
44.212822	-76.225695	28.44	28.5	150	2.2	1.32	5
44.214208	-76.229685	25.01	25.3	150	2.5	1.5	6
44.192515	-76.43862	28.52	28.7	150	2.19	1.31	6
44.159425	-76.363905	29.08	29	205	2.15	1.76	6
44.159517	-76.364318	25.46	26.7	205	2.45	2.01	5
44.165933	-76.372513	47.9	47.5	210	1.3	1.1	5
44.16617	-76.371973	46.45	41.1	210	1.35	1.13	3
44.12826	-76.389142	9	8.9	365	6.94	10.14	6
44.128235	-76.38925	8.7	8.75	365	7.18	10.49	6
44.122428	-76.460133	33.76	33.5	150	1.85	1.11	5
44.126375	-76.459342	18.61	17	180	3.36	2.42	5
44.124422	-76.450118	33.09	33.3	190	1.89	1.44	6
44.124292	-76.45021	36.95	37	190	1.69	1.29	6
44.184002	-76.46295	36.33	38.67	195	1.72	1.34	2
44.18437	-76.46318	31.15	30.5	195	2.01	1.57	3
44.223657	-76.391532	8.72	8.75	150	7.17	4.3	5
44.2237	-76.391447	8.84	8.9	150	7.07	4.24	6
44.223687	-76.391493	8.77	8.8	150	7.13	4.28	2
44.205173	-76.406322	12.75	12.75	220	4.9	4.31	6
44.204977	-76.406935	11.77	11.88	220	5.31	4.67	6
44.205207	-76.406432	12.54	12.5	220	4.98	4.39	5
44.212668	-76.265572	5.48	5.8	295	11.41	13.46	5
44.212932	-76.26589	10.64	10.6	295	5.87	6.93	6
44.212902	-76.265768	10.68	10.65	295	5.85	6.91	6
44.213498	-76.32	10.71	11.22	240	5.84	5.6	5
44.212935	-76.32086	11.88	12	240	5.26	5.05	4
44.21903	-76.367122	13.5	13.3	290	4.63	5.37	2
44.219155	-76.367047	14.71	14.4	290	4.25	4.93	5
44.205047	-76.40671	12.74	13	220	4.91	4.32	3
44.205212	-76.406552	12.88	12.85	220	4.85	4.27	3
44.2138283	-76.320445	11.68	11.22	240	5.35	5.14	4
44.2135533	-76.320048	11.87	11.15	240	5.27	5.05	4
44.2135567	-76.32003	10.22	11.07	240	6.12	5.87	3

Table 5.1: Summary of most relevant values for this study. A more detailed version of this table can be found in $data_summary_tables.zip$